Phase-coherent, injection-seeded, table-top soft-X-ray lasers at 18.9 nm and 13.9 nm

Y. WANG[1], E. GRANADOS[1], F. PEDACI[1], D. ALESSI[1], B. LUTHER[1], M. BERRILL[1] AND J. J. ROCCA[1,2]*

[1]National Science Foundation Engineering Research Center for Extreme Ultraviolet Science and Technology and Department of Electrical and Computer Engineering, Colorado State University, Fort Collins, Colorado 80523, USA

[2]Department of Physics, Colorado State University, Fort Collins, Colorado 80523, USA

*e-mail: rocca@engr.colostate.edu

Published online: 20 January 2008; doi:10.1038/nphoton.2007.280

There is keen interest in generating intense, coherent, soft-X-ray beams for scientific and measurement applications[1]. Here, we report the demonstration of soft-X-ray lasers with essentially full spatial and temporal coherence operating at wavelengths below 20 nm, and in particular within the 13-nm spectral region, which is important for the manufacturing of computer chips using extreme uv lithography. Gain-saturated pulses were produced in dense laser-created plasmas by amplifying high-harmonic seed pulses in the 18.9-nm and 13.9-nm transitions of nickel-like molybdenum and silver ions, respectively. These results, obtained using an injection seeding technique that can also be applied to improve the temporal coherence of free-electron lasers, extend our ability to generate bright phase-coherent laser beams to significantly shorter wavelengths. Moreover, the experiments were conducted using a practical table-top laser[2]. These compact soft-X-ray lasers offer new scientific opportunities, such as high-resolution coherent imaging and phase-coherent probing of atomic and molecular systems, in small laboratory environments.

Recently, a free-electron laser based on a large electron accelerator has produced extremely bright laser pulses with full spatial coherence at a fundamental wavelength of 13.7 nm (ref. 3). However, because the beam grows from spontaneous emission noise, its temporal coherence is, at present, limited by the emission of random uncorrelated phase wavetrains. The amplification of spontaneous emission from highly charged ions in plasma-based soft-X-ray laser (SXL) amplifiers can generate very monochromatic high-energy pulses, but with typically low coherence[4–7]. Recent results include the demonstration of a 13.2-nm table-top laser operating at 5 Hz (refs 2, 8). However, as this laser is also self-seeded by spontaneous emission noise, it has limited coherence.

Coherent high-harmonic (HH) pulses[9–11] can be amplified in population inversions created in dense plasmas while preserving many of their properties. Therefore, injection seeding of SXL amplifiers with HH pulses can generate intense soft-X-ray pulses with extremely high spatial coherence, low divergence, short pulsewidth and defined polarization. Furthermore, the very narrow linewidth of the plasma amplifier can increase the temporal coherence of the seed pulse. An early experiment demonstrated the amplification of HH pulses in a neon-like gallium plasma pumped by 600-J optical laser pulses, but only by a factor of three[12]. More recently, an optical field ionization SXL amplifier produced by femtosecond laser excitation of a krypton gas cell was seeded with the 25th harmonic of a Ti:sapphire laser to generate saturated amplification in the 32.8-nm laser line of nickel-like krypton (refs 13, 14). Our group has demonstrated the saturated amplification of HH seed pulses in the 32.6-nm line of neon-like titanium in a significantly denser transient collisional SXL plasma amplifier created by heating a solid titanium target[15]. Also recently, a neon-like manganese SXL medium was reported to amplify a HH seed from 4.7 pJ to 3 nJ (ref. 16). The seeding of this type of higher density, laser-heated solid target SXL amplifier, which has an increased saturation intensity and broader laser linewidth, should lead to phase-coherent lasers with higher intensities and shorter pulsewidths. However, so far, gain-saturated SXLs with high spatial and temporal coherence have been limited to wavelengths greater than 32 nm.

Here we report the first demonstration of essentially fully coherent SXLs at wavelengths below 20 nm and in the technologically important 13-nm spectral region of interest for extreme UV lithography metrology, and discuss the seed pulse amplification dynamics based on model simulations. The results were obtained by injection seeding, with HH pulses, collisionally excited SXL amplifiers operating in the $4d^1S_0-4p^1P_1$ transitions of nickel-like molybdenum and silver at 18.9 nm and 13.9 nm, respectively. Moreover, our experiments were conducted using a table-top laser with 5 Hz repetition rate, showing that this is a practical scheme to produce high-brightness SXL beams for applications in small laboratory environments.

The HH pulses from a Ti:sapphire laser were injected into SXL plasma amplifiers pumped by intense optical laser pulses impinging at a grazing incidence angle on a solid target, as illustrated schematically in Fig. 1. The spectra in Fig. 2 illustrate the dramatic improvement in laser beam divergence and intensity obtained by seeding a 2.5-mm-long 18.9-nm nickel-like molybdenum amplifier with pulses from the 43rd harmonic. The beam produced by the unseeded SXL amplifier (Fig. 2a) has a divergence of ~10 mrad. Figure 2b shows that the harmonic seed beam (shown with ×100 magnification) has a much smaller divergence, ~1.2 mrad. Seeding of the SXL amplifier results in a very small divergence, ~0.7 mrad, and a greatly increased intensity (Fig. 2c). Similar results were obtained when seeding

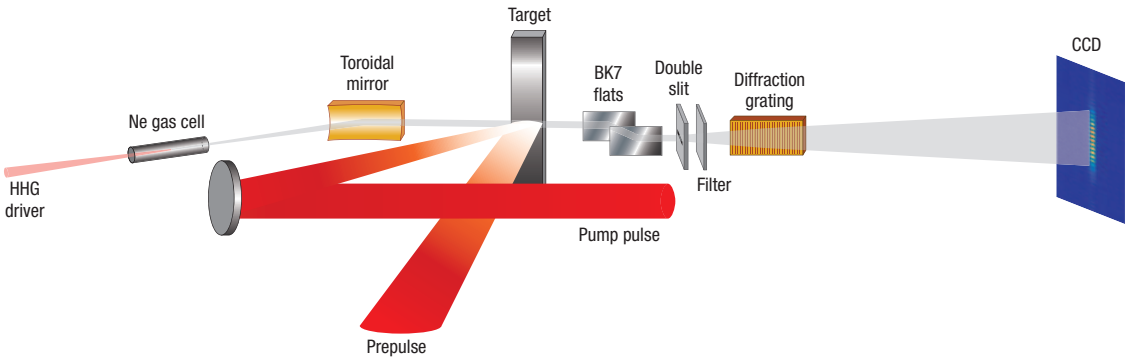

Figure 1 Schematic diagram of the injection-seeded, nickel-like SXL. The main optical laser pulse exciting the amplifier impinges at 23° grazing incidence onto the target. A neon gas cell is used to generate the high harmonic seed. The set-up used to measure the spatial coherence is shown to the right of the amplifier. HHG stands for high harmonic generation.

the isoelectronic transition in nickel-like silver at 13.9 nm with the 59th harmonic, as illustrated in Fig. 3. The increase in the energy of the seed pulse as a function of molybdenum plasma length is shown in Fig. 2d. Overall, the energy of the injected seed pulse is amplified more than 400 times. The most intense amplified pulses were measured with an energy of ~75 nJ. The fluence of these pulses significantly exceeds the computed saturation fluence of the 18.9-nm laser line of nickel-like molybdenum in these plasma conditions, $\sim 1.8 \times 10^{-3}\,\mathrm{J\,cm^{-2}}$. Because the nickel-like silver amplifier was operated at a slightly smaller gain, saturation occurs later within the amplifier, after a length of ~3 mm (Fig. 3d). Strong amplification is observed over a narrow range of time delays, ~1–1.5 ps between the peak of the short pump pulse and the arrival of the seed pulse (inserts of Figs 2d and 3d), which is compatible with a full-width at half-maximum (FWHM) gain duration of 4–6 ps.

The variation of the seed intensity and pulse shape as it propagates along the amplifier is initially governed by a dramatic narrowing of its bandwidth, which is not supported by the much narrower amplifier linewidth, and later, by saturation of the gain. The seed amplification was studied using a fully transient three-dimensional propagation code, developed in-house, that self-consistently computes its intensity increase and the gain saturation due to population inversion depletion by both the amplified spontaneous emission and the amplified seed pulse. The plasma parameters and the gain were calculated with a 1.5-dimensions lagrangian hydrodynamic/atomic physics code, in which the populations are determined by transient collisional-radiative calculations with radiation transport (Berrill, M. and Rocca, J. J., unpublished; see also Supplementary Information, Figs S1–S5). The computations show that the amplifier bandwidth contains similar contributions from collisional broadening ($\Delta\nu = 0.8 \times 10^{12}\,\mathrm{s^{-1}}$) and Doppler broadening ($\Delta\nu = 1.2 \times 10^{12}\,\mathrm{s^{-1}}$). However, the lorentzian component dominates in determining the amplified pulse width owing to its long tails. The computed increase in the seed pulse energy reproduces well the measured amplification behaviour well, as shown in Fig. 4 for the 13.9-nm nickel-like silver line. In the first 2 mm of the amplifier the seed bandwidth dramatically narrows (left inset panel in Fig. 4). This is accompanied by a very moderate energy increase, as only a small fraction of the initially broad bandwidth seed pulse is being amplified. This initial amplification phase, which concludes when the bandwidth of the seed approaches the linewidth of the amplifier, is followed by a rapid quasi-exponential growth, which terminates when the

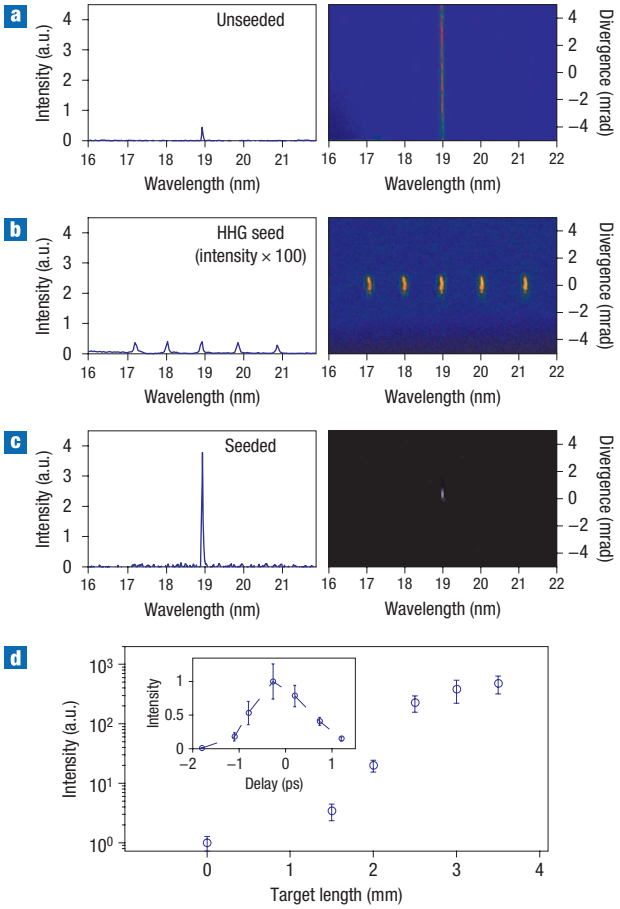

Figure 2 Characterization of seeded 18.9-nm nickel-like molybdenum laser. **a**–**c**, Spectra illustrating the dramatic improvement in the beam divergence and beam intensity achieved by seeding an 18.9-nm nickel-like molybdenum SXL amplifier with a high harmonic pulse: unseeded SXL amplifier (**a**); HH seed (**b**); seeded SXL amplifier (**c**). The length of the plasma amplifier is 2.5 mm. The intensity scale of the seed pulse is magnified 100 times. **d**, Measured variation of the amplified HH seed pulse energy as a function of plasma amplifier length. The seed pulses reach the gain saturation intensity after propagating ~2.5 mm into the SXL amplifier. The insert shows the intensity of the amplified pulse as a function of delay between the peak of the heating pulse and the arrival of the seed pulse. The error bars correspond to the standard deviation of 10–20 laser shots.

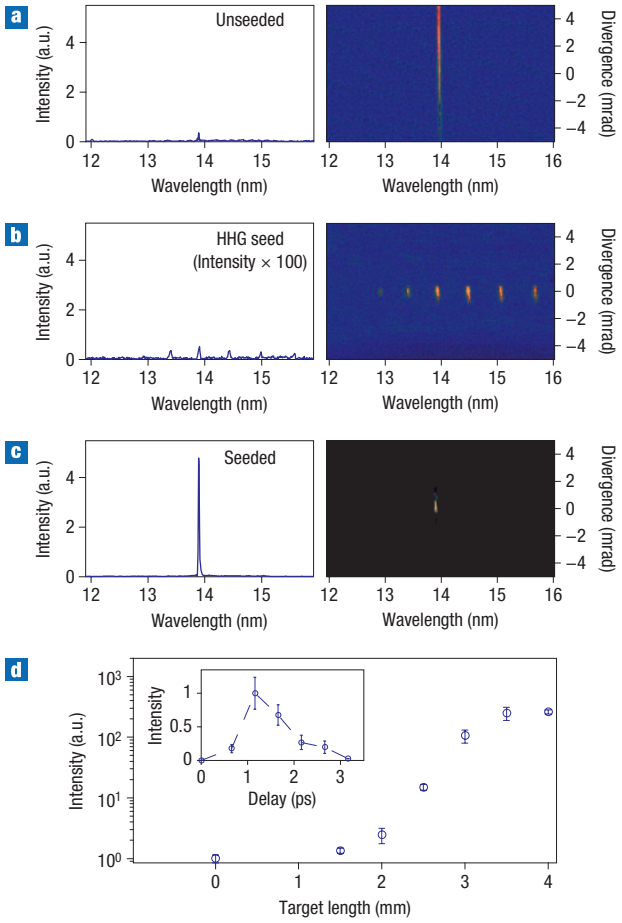

Figure 3 Characterization of seeded 13.9-nm nickel-like silver laser. **a**–**c**, Spectra illustrating the relative intensity and beam divergence for different set-ups an injection-unseeded SXL laser amplifier (**a**); HH seed (intensity scale magnified ×100) (**b**); seeded SXL amplifier (**c**). The length of the plasma amplifier is 3 mm. **d**, Measured variation of the amplified HH seed pulse energy as a function of the plasma amplifier length. The insert shows the intensity of the amplified pulse as a function of delay between the peak of the heating pulse and the arrival of the seed pulse. The error bars correspond to the standard deviation of 10–20 laser shots.

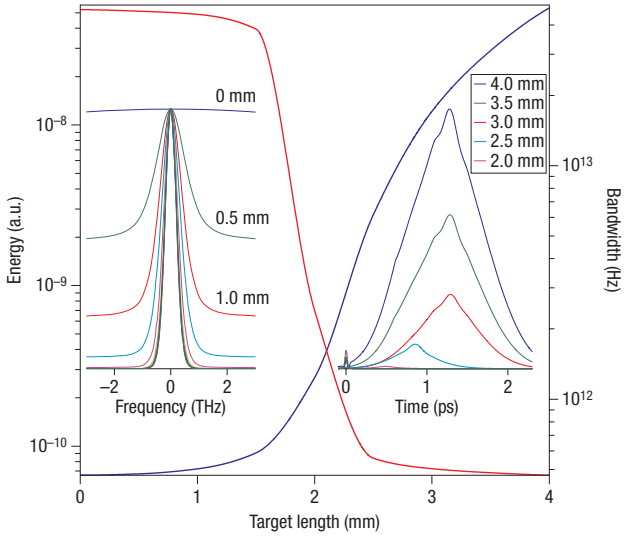

Figure 4 Computed variation of the intensity, bandwidth, spectrum and pulse shape of the seeded 13.9-nm laser pulse as a function of the nickel-like silver amplifier length. The left insert illustrates the rapid narrowing of the normalized spectrum as the seed pulse is amplified along the plasma column. In the main graph, the red curve describes the corresponding variation of the spectral bandwidth, defined for the purpose of this figure as the spectral width containing 76% of the pulse energy. This bandwidth decrease is accompanied by a slow initial increase of the pulse intensity, which is followed by a quasi-exponential increase that tapers when the saturation fluence is reached (blue curve). The insert on the right illustrates the evolution of the laser pulse shape, which is characterized by rapid initial width increase due to the amplifier bandwidth limitations, and by slight asymmetries caused by gain saturation. The amplified pulse is preceded by a short pulse of nearly constant intensity composed of the broad spectrum of non-amplified frequencies.

saturation fluence is reached, at an amplifier length of about 2.5 mm. The corresponding temporal profile of the amplified seed pulse is characterized by a rapid initial width increase due to the amplifier bandwidth limitations, followed by gain saturation broadening (right in Fig. 4). The amplifier bandwidth is computed to sustain pulses of 0.8–0.9 ps FWHM duration. However, additional pulse broadening, in this case to ~1.0 ps, can result from operating the amplifier significantly above its saturation fluence. Owing to a slower group velocity caused by the gain, the amplified pulse follows a short pulse containing the non-amplified frequencies of the injected seed, which propagates with a group velocity nearly equal to the speed of light in vacuum. As the pulse duration is predominantly determined by the lorentzian component of the amplifier linewidth, operation at a higher plasma density will result in a nearly inversely proportional pulsewidth. For example, injection seeding of a plasma amplifier with a density of 2.5×10^{21} cm^{-3} can potentially allow the generation of sub-100-fs soft-X-ray laser pulses. Recently, a promising approach to studying this problem using Maxwell–Bloch simulations was published, but at present this approach does not include a fully transient treatment of the level populations[17].

The spatial coherence of the unseeded and injection-seeded lasers was determined in a Young's double-slit interference experiment measuring the fringe visibility as a function of slit separation. Figure 5a–d shows single-shot interferograms and their profile lineouts for the seeded 18.9-nm nickel-like molybdenum laser. The interferogram corresponding to the 30-μm slit pair shows full fringe visibility. Figure 5e shows the variation of the maximum measured fringe visibility as a function of slit separation for both the unseeded and the seeded nickel-like molybdenum lasers. To characterize the spatial coherence length we use the coherence radius R_c (ref. 18), within which the fringe visibility is larger than 0.61. Assuming a gaussian profile, R_c of the unseeded laser is ~50 μm, which is only a very small fraction of the ~1-mm beam diameter at this location. Therefore, only a very small part of the unseeded laser pulse energy is contained within the region where the beam is spatially coherent. In contrast, for the seeded laser $R_c = 84$ μm, a value practically equal to the 80–100 μm beam diameter, indicating a very high degree of spatial coherence through nearly the entire beam. The degree of spatial coherence of the seeded 13.9-nm nickel-like silver laser was measured to be practically identical to that of the seeded 18.9-nm molybdenum laser. This extraordinarily high degree of spatial coherence is accompanied by very high temporal coherence. Although phenomena such as ionization of the HH media and the rapid intensity-dependent variation of the HH phase in the single-atom response can

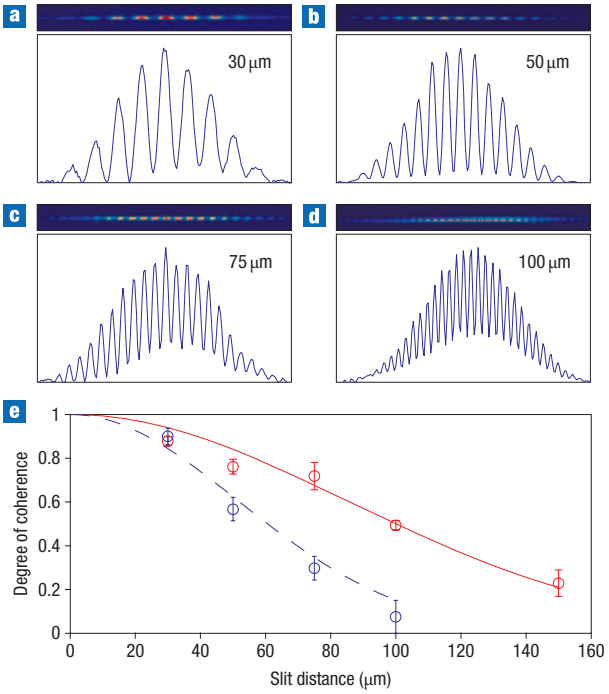

Figure 5 Single-shot interferograms of the seeded nickel-like molybdenum 18.9-nm laser beam for different slit separations. a–d, Two-slit interferograms and corresponding intensity lineouts. The slit pairs were placed 10 cm from the exit of the SXL amplifier. In the right-hand side of the 30-μm interferogram, the visibility is degraded by uneven illumination of the slits. **e**, Degree of coherence $|\mu_{12}(\Delta x)|$ as a function of slit separation for the injection-seeded (solid line) and unseeded (dashed line) laser. Error bars illustrate the variation of the degree of coherence for three interferograms. The lines are gaussian profiles for $R_c = 50$ μm (unseeded) and $R_c = 84$ μm (seeded). It is important to note that the laser beam diameters at this location are 80–100 μm and ~1 mm for the seeded and unseeded lasers, respectively.

degrade the temporal coherence of the injected seed[19], the very narrow bandwidth of the amplifier ($\Delta\lambda/\lambda \approx 6 \times 10^{-5}$) greatly limits any frequency chirp, effectively enabling the generation of a pulse with very high temporal coherence.

These characteristics, combined with the small source size, define a very high peak spectral brightness, estimated to be between 0.2×10^{26} and 2×10^{26} photons per (s mm^2 mrad^2 0.01% bandwidth). Within 0.01% of the bandwidth, the peak spectral brightness is about three orders of magnitude smaller than that of the recently demonstrated 13.7-nm free-electron laser, and exceeds third-generation synchrotrons by between four and five orders of magnitude[3]. Increases in the plasma amplifier volume and density would further increase the brightness. The uniquely narrow bandwidth is an advantage for applications such as coherent imaging.

In summary, we have demonstrated phase-coherent table-top SXLs with low divergence at wavelengths as short as 13.9 nm. These bright sources will lead to opportunities to realize new applications of phase-coherent SXL light at relevant wavelengths on a table top.

METHODS

INJECTION-SEEDED SOFT-X-RAY AMPLIFIER

Pulses produced by a single 815-nm wavelength table-top chirped pulse amplification Ti:sapphire laser system were used for both generating the harmonic seed pulses and to pump the SXL amplifiers. The amplifiers consist of plasmas created by irradiating polished molybdenum or silver slabs up to 4 mm in length with a sequence of a 10-mJ prepulse with a duration of 120 ps, followed after about 5 ns by a second prepulse of the same duration and ~350 mJ energy, impinging at normal incidence. The use of an early low-energy prepulse assists in the creation of a smooth plasma with a larger gain region and reduced density gradients. The second prepulse heats the plasma, increasing the degree of ionization to approach the nickel-like stage. This pulse was in turn followed after 700 ps (for molybdenum) or 300 ps (for silver) by a 6.7-ps heating pulse of ~0.9-J energy, impinging at a grazing incidence angle of 23°, which rapidly heats the plasma giving rise to a transient population inversion. The grazing incidence pumping geometry takes advantage of pump-beam refraction to increase its energy deposition in the plasma region with optimum density for amplification[20,21]. The 23° angle was selected to couple the pump beam into the region where the plasma density is $\sim 2.6 \times 10^{20}$ cm^{-3}. The prepulses were focused into a 30-μm-wide, 4.1-mm FWHM long line focus using a combination of a spherical lens and a cylindrical lens. The short pulse was focused into a similar line focus using a parabolic mirror with a focal length of 76.2 cm positioned at 7° from normal incidence. The off-axis placement of the paraboloid formed an astigmatic focus that resulted in a line that was further elongated to 4.1 mm when intercepted at grazing incidence by the target. The 20-mJ laser pulses used to drive the HH generation were compressed to about 50 fs using a separate grating compressor, and focused on the input of the neon gas cell with a 5-m focal length lens. The gas cell consists of a stainless steel tube 4 cm in length, with entrance and exit orifices of 700 μm, filled with 20 torr of neon. The HH output of the gas cell was relay imaged onto a ~100-μm-diameter spot at the input of the plasma amplifier using a gold-coated toroidal mirror designed to operate at a grazing incidence angle of 10°. The wavelength of the selected harmonic order was made to overlap with that of the laser line by tuning a thin etalon introduced in the first of the three multipass amplifiers of the Ti:sapphire laser system. Maximum seeded amplification was observed when injecting the HH seed pulses at ~5.5 mrad grazing angle with respect to the target surface. This angle optimizes the trajectory of the seed beam through the gain medium in the presence of beam refraction created by the density gradient. Two BK7 windows positioned at 9° grazing incidence and sets of either two or three thin-film filters (0.3-μm- and 0.5-μm-thick aluminium for the molybdenum laser, and 0.3-μm-thick zirconium for the silver laser) were used to attenuate the straight light from the 815-nm beam used to generate the high harmonics. The output of the soft-X-ray amplifier was dispersed with a variable-space diffraction grating (nominal line spacing 1,200 lines mm^{-1}) and was detected by a back-thinned CCD.

SPATIAL COHERENCE MEASUREMENTS

The modulus of the normalized complex degree of coherence μ_{12} is proportional to the the fringe visibility, defined as $V = (I_{max} - I_{min})/(I_{max} + I_{min})$, where I_{max} and I_{min} are the maximum and minimum intensities of the fringe pattern. Maximum visibility requires uniform illumination of the slits. Pairs of 5-μm-wide slits with separations ranging from 30 μm to 150 μm were placed 10 cm from the exit of the plasma amplifier, where the FWHM beam diameter is 80–100 μm. The interference pattern was recorded with a 2,048 × 2,048 pixel back-illuminated CCD camera, using a set-up similar to that used for the rest of the measurements, in which the residual 815-nm beam was attenuated with a pair of grazing incidence BK7 windows and one aluminium or zirconium filter. The background plasma light was dispersed with a diffraction grating. The degree of coherence is undervalued, as the data, which were obtained at a short distance from the amplifier exit, contain a contribution from the significantly less coherent and more divergent amplified spontaneous emission light.

The van Cittert–Zernike theorem can be used to estimate the size of an incoherent source having the same degree of spatial coherence[1]. The equivalent incoherent source size was found to be 7 μm and 5.3 μm for the molybdenum and silver seeded lasers, respectively. The effective source sizes can be estimated by convoluting these values with the FWHM diameter of a gaussian beam corresponding to the measured divergence. Assuming a gaussian intensity distribution, the source size can be estimated to be 13 μm and 10 μm for the molybdenum and silver seeded lasers, respectively. However, if the beam profile is flatter owing to the stronger saturation of the gain on-axis and the overfilling of the gain region by the harmonic seed, the spot size could be larger, ~28 μm (molybdenum) and ~21 μm (silver) in the limit case of a flat-top profile.

Received 30 September 2007; accepted 16 November 2007; published 20 January 2008.

References

1. Attwood, D. T. *Soft X-Rays and Extreme Ultraviolet Radiation: Principles and Applications* (Cambridge Univ. Press, Cambridge, 1999).
2. Wang, Y. *et al.* Demonstration of high-repetition-rate tabletop soft-X-ray lasers with saturated output at wavelengths down to 13.9 nm and gain down to 10.9 nm. *Phys. Rev. A* **72,** 053807 (2005).
3. Ackermann, W. *et al.* Operation of a free-electron laser from the extreme ultraviolet to the water window. *Nature Photon.* **1,** 336–342 (2007).
4. Amendt, P., Strauss, M. & London, R. A. Plasma fluctuations and X-ray laser transverse coherence. *Phys. Rev. A* **53,** R23–R26 (1996).
5. Tang, H. *et al.* Spatial coherence measurement of 13.9 nm Ni-like Ag soft X-ray laser pumped by a 1.5 ps, 20 J laser. *Jpn J. Appl. Phys.* **42,** 443–448 (2003).
6. Lucianetti, A. *et al.* Transverse spatial coherence of a transient nickel-like soft X-ray laser pumped by a single picosecond laser pulse. *Opt. Lett.* **29,** 881–883 (2004).
7. Liu, Y. *et al.* Spatial coherence measurements of a 13.2 nm transient nickel-like cadmium soft X-ray laser pumped at grazing incidence. *Opt. Express* **14,** 12872–12879 (2006).
8. Rocca, J. J. *et al.* Saturated 13.2 nm high-repetition-rate laser in nickel-like cadmium. *Opt. Lett.* **30,** 2581–2583 (2005).
9. Kapteyn, H. C., Murmane, M. M. & Christov, I. P. Extreme nonlinear optics: Coherent X-rays from lasers. *Phys. Today* **58,** 39–44 (2005).
10. Zhang, X. *et al.* Highly coherent light at 13 nm generated by use of quasi-phase-matched high-harmonic generation. *Opt. Lett.* **29,** 1357–1359 (2004).
11. Nagata, Y., Furusawa, K., Nabekawa, Y. & Midorikawa, K. Single-shot spatial coherence measurements of 13 nm high order harmonic beam by a Young's double slit measurement. *Opt. Lett.* **32,** 722–724 (2007).
12. Ditmire, T. *et al.* Amplification of XUV harmonic radiation in a gallium amplifier. *Phys. Rev. A* **51,** R4337–R4340 (1995).
13. Zeitoun, P. *et al.* A high-intensity highly coherent soft X-ray femtosecond laser seeded by a high harmonic beam. *Nature* **431,** 426–429 (2004).
14. Mocek, T. *et al.* Absolute time-resolved X-ray laser gain measurement. *Phys. Rev. Lett.* **95,** 173902 (2005).
15. Wang, Y. *et al.* High-brightness injection-seeded soft-X-ray-laser amplifier using a solid target. *Phys. Rev. Lett.* **97,** 123901 (2006).
16. Kawachi, T. *et al.* Recent progress in X-ray laser research at JAERI. *Proc. SPIE* **5919,** 155–165 (2005).
17. Al'miev, I. R. *et al.* Dynamical description of transient X-ray lasers seeded with high-order harmonic radiation through Maxwell–Bloch numerical simulations. *Phys. Rev. Lett.* **99,** 123902 (2007).
18. Goodman, J. W. *Statistical Optics* 171–187 (Wiley, New York, 1985).
19. Bellini, M. *et al.* Temporal coherence of ultrashort high-order harmonic pulses. *Phys. Rev. Lett.* **81,** 297–300 (1998).
20. Keenan, R. *et al.* High-repetition-rate grazing-incidence pumped X-ray laser operating at 18.9 nm. *Phys. Rev. Lett.* **94,** 103901 (2005).
21. Luther, B. M. *et al.* Saturated high-repetition-rate 18.9-nm tabletop laser in nickellike molybdenum. *Opt. Lett.* **30,** 165–167 (2005).

Acknowledgements

We thank Yanwei Liu and D. Attwood for discussions concerning the coherence properties of these lasers. We also gratefully acknowledge the contribution of M. Larotonda and useful discussions with H. Kapteyn and M. Murnane. This work was supported by the National Science Foundation (NSF) Engineering Research Center programme (NSF Award EEC-0310717). M.B. acknowledges a Department of Energy fellowship (DE-FG02-97ER25308).
Correspondence and requests for materials should be addressed to J.J.R.
Supplementary information accompanies this paper on www.nature.com/naturephotonics.